J Neurol (2010) 257:271–280
DOI 10.1007/s00415-009-5307-z

ORIGINAL COMMUNICATION

Bilateral brainstem activation by thermal stimulation of the face in healthy volunteers

Bärbel Kubina · Dejan Ristić · Jochen Weber · Christian Paul Stracke · Clemens Forster · Jens Ellrich

Received: 31 March 2009 / Revised: 18 August 2009 / Accepted: 25 August 2009 / Published online: 13 September 2009

Abstract Contralateral sensory deficits in Wallenberg's lateral medullary syndrome suggest bilateral processing of trigeminal afferent input in the human brainstem. On the basis of experiments in rodents and clinical data, the present study addresses the hypothesis of bilateral projection of facial nociceptive input onto the spinal trigeminal nucleus (STN) in healthy humans. Nociceptive processing in the brainstem was investigated by functional magnetic resonance imaging (fMRI) in 18 healthy volunteers. Heat stimuli (39, 43, 46°C) were applied by a Peltier type thermode to the left forehead (V1) and the left mental region (V3). Analyses of fMRI data were performed with SPM2 and BrainVoyager software. A region-of-interest approach analyzed local activation in the STN. Heat evoked significant bilateral activation in the STN ($P < 0.01$, $T > 2.8$). Contralateral activation was more frequent during stimulation of the V1 than of the V3 region. Whereas activation by V1 stimulation was located in caudal STN, V3 stimulation induced activity in more rostral parts of the STN. Functional MRI data in humans suggest bilateral brainstem activation when heat is applied to the face. Contralateral brainstem activity is more pronounced by stimulation of V1 as compared to V3. The results indicate similar nociceptive processing in humans and rodents and may explain clinical findings.

Keywords Brainstem · Orofacial · Pain · Trigeminus

D. Ristić · J. Ellrich (✉)
Medical Physiology and Experimental Pharmacology Group, Center for Sensory-Motor Interaction, Department of Health Science and Technology, Medical Faculty, Aalborg University, Fredrik Bajers Vej 7D2, 9220 Aalborg, Denmark
e-mail: jellrich@hst.aau.dk

B. Kubina
Experimental Neurosurgery Section, Department of Neurosurgery, RWTH Aachen University, Aachen, Germany

J. Weber
Brain Innovation B.V., Maastricht, The Netherlands

J. Weber
Social Cognitive Affective Neuroscience Unit, Department of Psychology, Columbia University, New York, USA

C. P. Stracke
Department of Neuroradiology, Alfried Krupp Hospital Essen, Essen, Germany

C. Forster
Institute for Physiology and Experimental Pathophysiology, University of Erlangen-Nuremberg, Erlangen, Germany

Introduction

Diminished pain and temperature perception on the ipsilateral face and contralateral body is the classical feature of Wallenberg's lateral medullary syndrome (WLMS) [58]. However, a neuropathological report (autopsy) on a patient with a demyelination in the dorsolateral medulla oblongata documented diminished pain and temperature perception in the contralateral face [51]. Triggered by this case report, some studies addressed the spatial distribution of sensory loss in the face in lateral medullary infarction (LMI) as confirmed by magnetic resonance imaging (MRI). In 13 patients with LMI, six suffered from total or partial loss of pain and temperature sensation in the contralateral face [8]. Of 130 LMI patients, 25% showed contralateral and bilateral dysfunction, while 14% had sensory dysfunction on the

face [28]. A clinical study with 117 patients suffering from LMI detected contralateral sensory dysfunctions in the face in 18% [27]. Correspondingly, in approximately 20% of LMI patients, somatosensory functions in the contralateral face are impaired. The affection of the contralateral face seems to have an impact on the development of central poststroke pain (CPSP) in LMI [35]. CPSP developed in 16 of 63 LMI patients within 6 months of the infarct. The most common site for the pain was around the eye ipsilateral to the infarct. The presence of CPSP could be predicted with 100% specificity and 89% sensitivity by the demonstration of normal thresholds to heat and pressure pain stimulation from the cheek contralateral to the side of the infarct. Thus, normal pain processing in the contralateral face strongly predicts CPSP. Considering an incidence of 25% for CPSP in LMI, the results imply contralateral hypoalgesia in the majority of patients without CPSP.

The occurrence of contralateral sensory loss in LMI may be due to involvement of the contralateral trigeminothalamic tract that crosses to the side of lesion within the dorsolateral medulla oblongata [9, 42]. Alternatively, neurons within the spinal trigeminal nucleus (STN) may receive afferent input from the contralateral face as demonstrated by electrophysiological and histological studies in rodents [16, 23, 38].

The present study addresses the hypothesis of bilateral projections from nociceptive afferent fibers in the face onto the STN in the brainstem of human volunteers by applying functional magnetic resonance imaging (fMRI). Preliminary results of the human experimental study were presented as an oral communication at the fourth international meeting of the BrainStem Society [32].

Methods

The experiments were conducted in 11 female and 8 male healthy volunteers aged 21–31 years (24 ± 2.5 years, mean ± standard error). Three participants were left handed. All gave their informed consent to the study according to the Declaration of Helsinki, 1964 (as amended by the 52nd General Assembly, Edinburgh, Scotland, 2000; http://www.wma.net). The protocol was approved by the local ethics committee. Drug usage and neurological disorders as well as ferromagnetic implants served as exclusion criteria. Before starting the trial, the experimental protocol was explained to the subjects in detail. During functional imaging, subjects were instructed to lie still and keep their eyes closed. The volunteers could stop the experiment at any time by pressing a safety button.

In general, noxious heat stimuli were applied to left innervation territories of the supraorbital nerve (V1) at the forehead and the mental nerve (V3) at the chin in healthy volunteers. Changes of neuronal activity in brainstem structures due to 39, 43, and 46°C stimuli were monitored via fMRI. The scanned brainstem structures covered the upper cervical spinal cord up to the midbrain.

Temperature thresholds

At the beginning of the experiment, individual warm detection threshold (WDT) and heat pain threshold (HPT) were determined in order to provide for normative values in all subjects included in the study. Temperature stimuli were applied to left V1 and V3 regions (see above) by a 1.6×1.6 cm^2 computer controlled Peltier type thermode (TSA-II NeuroSensory Analyzer, Medoc Advanced Medical Systems Ltd., Ramat-Yishai, Israel). This non-ferromagnetic thermode is specially adapted to be used in MRI including a radiofrequency filter. Starting from a baseline temperature of 32°C, temperature was increased by 1°C/s up to a maximum of 50°C. The volunteers were asked to press a computer mouse button as soon as they detected the corresponding temperature sensations warmth or heat pain, respectively. After pressing the mouse button, the temperature was allowed to return to the baseline temperature. The arithmetic mean of four WDT and three HPT threshold values were calculated. WDT is given as the difference in temperature from baseline (dT) and HPT as the absolute temperature (°C).

Thermal test stimulation

Corresponding to measurement of the superficial skin temperature at the forehead and the chin (see above), the baseline temperature of the thermode was adjusted to 34°C. The square thermode (1.6×1.6 cm^2) was placed 2 cm above the eyebrow and 2 cm lateral to the facial midline at the forehead. At the mandible, the thermode was placed 2 cm lateral to the facial midline and centered between the lower edge of the canine tooth and the base of the mandible. Three different temperatures were consecutively applied to the V1 or V3 area. Within one single thermal stimulus, temperature was increased from 34 to 39°C, 43, or 46°C, respectively, at a rate of 4°C/s and remained at that level for exactly 15 s before returning to baseline (Fig. 1). One thermal stimulation series consisted of ten identical test stimuli with an interstimulus interval of 30 s. The stimulation paradigm in one stimulation area started with ten thermal stimuli of 39°C, followed by ten stimuli of 43°C, and finally ten stimuli of 46°C (Fig. 1). Later during data analysis, the first temperature stimulation of one series was excluded from data analyses in order to assure a sufficient scanner signal equilibration and, thus, achieving higher data quality. C fiber nociceptors exhibit a lower heat threshold (usually <40°C) than Aδ fiber nociceptors

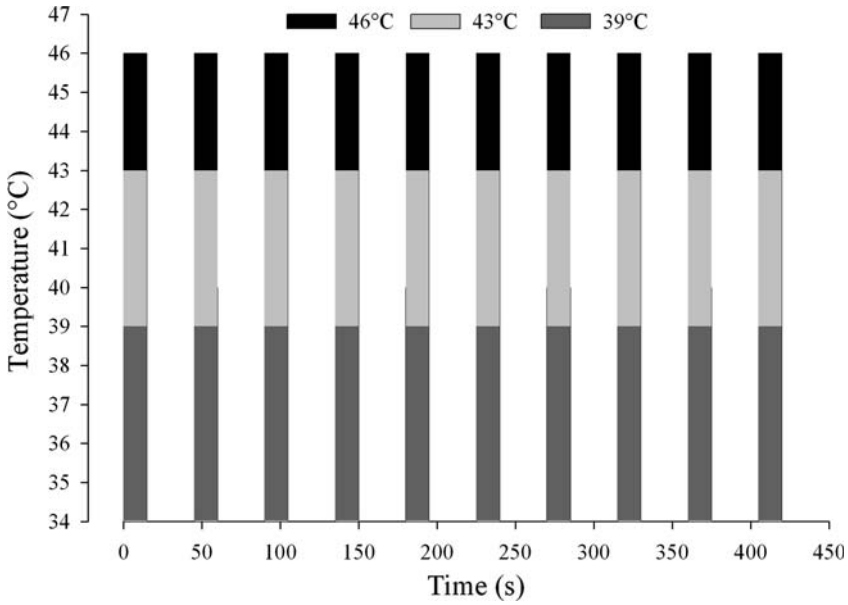

Fig. 1 Thermal stimulation paradigm. Thermal stimuli were consecutively applied to the left forehead (V1) and to the left chin (V3) by a computer-controlled Peltier thermode. Each thermal stimulus started from a baseline temperature of 34°C, heated up to 39, 43, or 46°C at a rate of 4°C/s, and remained at the corresponding temperature for exactly 15 s before cooling down to baseline. One thermal stimulation series consisted of ten identical heat pulses with an interstimulus interval of 30 s. In each area (V1, V3), three thermal stimulation series with 39, 43, and 46°C were applied

(always >42°C) [33, 55]. Accordingly, in the present study, thermal stimuli were adjusted to 39, 43, and 46°C in order to induce different peripheral noxious afferent input. Due to possible transient sensitization effects of 46°C stimulation, this temperature was applied last within a series. V1 and V3 stimulation were consecutively conducted in one experimental session. One experimental session lasted approximately 90 min.

MRI scanning

Functional MRI was performed utilizing a 1.5 T Philips Gyroscan NT Intera Achieva (Philips Medical Systems, Best, NL) with a standard linear neck coil. The head was fixed within the neck coil by foam cushions in order to minimize movement. Earplugs were used to reduce background noise and to prevent distraction.

A sagittal T1-weighted 3D gradient echo imaging sequence was used. The field of view (FOV) during anatomical and functional scanning covered the brainstem (spinal segment C1, medulla oblongata, pons, and midbrain) and measured a craniocaudal range of 140 mm. Anatomical images were acquired using a sagittal T1-weighted 3D fast field echo (FFE)–gradient echo sequence. Time of echo (TE) was 4.6 ms, time of repetition (TR) was 25 ms and the flip angle was 30°. The 256 × 256 matrix was reconstructed with 512 × 512. Thirty slices with a slice thickness of 2 mm were recorded without slice gaps. The acquired voxel size (ACQ) in multipath scanning (MPS) was 0.55 × 0.55 × 4 mm^3 and the reconstructed voxel size (REC) in MPS measured 0.27 × 0.27 × 2 mm^3.

Prior to performing functional imaging a homogenization of the magnetic field was done by volume shim. Thereafter, four dummy scans were performed. Functional images were recorded with multi-slice T2*-weighted FFE–gradient echo-echoplanar sequences (EPI) in single-shot technique using the same FOV. TE was 50 ms, TR 3,000 ms. Flip angle was 90°. Sixteen anterior to posterior sagittal slices were recorded with a thickness of 3 mm each and a slice gap of 0.1 mm. The matrix was set to 64 × 64 and reconstructed with 128 × 128. ACQ voxel in MPS were 2.19 × 2.22 × 3 mm^3 and REC voxel were 1.09 × 1.09 × 3 mm^3. Each stimulation series with 10 thermal stimuli each included 150 dynamic scans and lasted approximately 8 min. Accordingly, three stimulation series with different temperatures in one anatomical site (V1 or V3) produced 450 scans.

MRI data analysis

Functional data was processed with SPM2 (Statistical Parametric Mapping, Wellcome Department of Imaging Neuroscience, London, http://www.fil.ion.ucl.ac.uk/spm/) and BrainVoyager QX 1.9 (Brain Innovation B.V., Maastricht, The Netherlands, http://www.brainvoyager.com). Due to the required analysis of brainstem imaging data, the single subject analysis was performed by SPM2 and the group analysis by a combination of SPM2 and BrainVoyager QX. Thus, a brainstem template displaying ten distinct activation localizations could be established. Due to extensive movement, one subject was excluded from further data analysis.

Single subject analysis

Preprocessing of EPI images consisted of 3D realignment, which allowed maximal movements of 3 mm and 3° in each plain of the brainstem, coregistration of individual EPI images onto the individual anatomy, spatial smoothing

with a 2 mm FWHM Gaussian filter and a landmark-based normalization. Normalization of data was carried out with a custom-made algorithm. The following five landmarks were chosen: genu corporis callosi, interception point between sinus rectus and occipital flake, interception point between vena galeni and sinus rectus, fastigium cerebelli, and dens axis.

After specification of the experimental design and computation of β-errors, activation projected onto the individual anatomies was displayed. Minimal cluster size was set to 3 voxel (10.7 mm^3) [11, 36] with uncorrected $P < 0.02$ ($T > 2.06$) for activation in the pons and $P < 0.05$ ($T > 1.65$) in the medulla/spinal dorsal horn (SDH). Images were overlaid by anatomically corresponding drawings derived from two different brainstem atlases [12, 15]. Contrasts were calculated for each temperature. Activation clusters matching the indicated STN localization were included in the statistical analysis. Lacking a brainstem template, no spatial normalization and no further data analysis could be conducted with SPM2.

Group analysis (anatomical data)

A major obstacle for brainstem fMRI is the lack of a standardized 3D space template to transform the individual data to one standard brain. This procedure would also provide for clear localization of activations and statistical comparison of individual activation patterns. Analyzing cortical fMRI, the MNI glass brain and Talairach systems provide such a template [34]; therefore, an anatomical brainstem template was created using SPM2 (Fig. 2a). All 18 individual sets of anatomical images were compared concerning determined distances of landmarks. Among the 18 volunteers, one set of anatomical images with the least variation in anatomical structures (comparison of determined distances of landmarks) was defined as the median data set. All anatomical images were coregistered to the selected median set of anatomical images (Fig. 2a; 1). This approach provided for a temporary mean anatomical brainstem template by averaging (Fig. 2a; 2). All 18 coregistered anatomical sets were normalized to the temporary brainstem template (Fig. 2a; 3). These normalized anatomical images were averaged to the final anatomical template used for EPI processing (Fig. 2a; 4).

Group analysis (functional data)

Corresponding to the processing of anatomical data, functional images underwent a series of coregistration and normalization in order to fit onto the anatomical brainstem template created (see above). This procedure resulted in a group analysis with ten distinct activation localizations projected onto the anatomical template. After motion correction, functional scans were coregistered and normalized ($0.5 \times 0.5 \times 0.5$ voxel) to the anatomical template (Fig. 2b). Each functional scan was coregistered to its corresponding anatomy on an overlay (Fig. 2b; 1). Thus, normalization parameters used for the normalization of each individual anatomy with the brainstem template (Fig. 2b; 2) were applied to coregistered EPIs (Fig. 2b; 3). The resulting 18 sets of coregistered and normalized EPIs were used for further processing in the group analysis. Subsequently, the anatomical template and the pre-processed EPIs were imported into BrainVoyager. Equal bounding box parameters were used (BrainVoyager, bounding box: x axis 100–49, y axis 95–154, z axis 75–199) in order to keep images strictly in the same 3D space in both programs (SPM2: x and y axis -80 to $+79$, z axis -30 to $+29$). In BrainVoyager functional data were isovoxelated to $1 \times 1 \times 1$ mm^3 voxel and trilinearly interpolated (256×256 matrix). In addition, the very first temperature stimulation within a series of ten was excluded from data analyses in order to assure a sufficient scanner signal equilibration, thus, achieving higher data quality. Subsequently, group activation projected onto the anatomical template was visualized. Single temperatures and temperature contrasts of 43 minus 39°C as well as 46 minus 39°C were analyzed. Positive and negative BOLD signals were considered.

A region-of-interest (ROI) analysis was performed to select activation. The included clusters were localized in the rostral SDH, medulla oblongata or pons and had to have a dorsolateral position in the axial section. Activation clusters smaller than 2 voxel (2 mm^3) were excluded.

Statistical analysis

Clusters in single subject analysis were categorized into number of clusters and number of voxel each for the three anatomical regions (SDH, medulla, pons), ipsilateral and contralateral activation site, and V1 and V3 stimulation, respectively.

Statistical analysis was performed with SPSS (version 14.0, SPSS Inc., Chicago, IL, USA) and SigmaStat® (version 3.1, SPSS Inc., Chicago, IL, USA). The following statistical tests were applied: Friedman's test, multivariance analysis and normality test (Kolmogorov–Smirnov test), for non-parametric data the Mann–Whitney rank-sum test, one way repeated measures (RM) ANOVA on ranks, and for parametric data the paired t-tests and one- and two-way RM ANOVA.

Statistical group analysis included BrainVoyager's general linear model (GLM) with z-transformation, random effect analysis (RE) and for each ROI an ANOVA with $P < 0.01$ ($T > 2.8$). Significant clusters were categorized into anatomical localization, activation side, stimulation

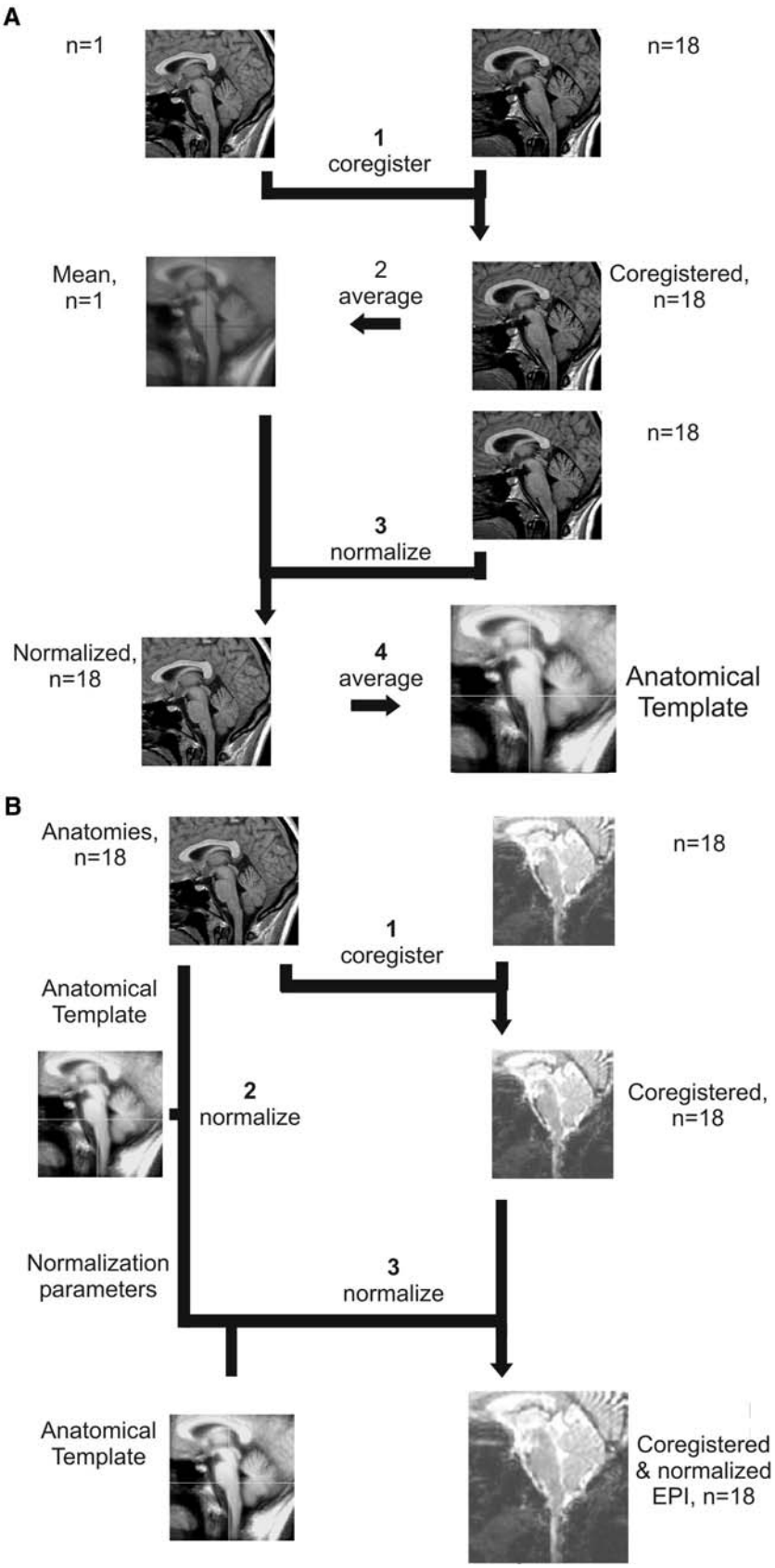

Fig. 2 Processing of anatomical and functional images. **a** Creation of the anatomical template. After comparison of determined distances of landmarks in all volunteers one set (out of 18) of anatomical images was defined as the median data set. All anatomical images were coregistered to the selected median set of anatomical images (*1*). This approach provided for a temporary mean anatomical brainstem template by averaging (*2*). All 18 coregistered anatomical sets were normalized to the temporary brainstem template (*3*). These normalized anatomical images were averaged to the final anatomical template used for EPI processing (*4*). **b** Processing of EPIs. Each functional scan was coregistered to its corresponding anatomy on an overlay (*1*). Thus, normalization parameters used for the normalization of each individual anatomy with the brainstem template (*2*) were applied to coregistered EPIs (*3*). The resulting 18 sets of coregistered and normalized EPIs were used for further processing in the group analysis

site, applied temperature, and activation as positive or negative BOLD response.

Matching of localizations

Statistically approved activations in group analysis underwent a second selection. Localization of clusters at a single temperature was compared with those displayed in temperature contrasts. This matching brought up ten distinct activation localizations where the majority of clusters were situated (all temperatures included). Clusters not matching these areas were excluded from the following second categorization (anatomical localization, activation side, stimulation site, applied temperature, and activation as positive or negative BOLD response).

Results

Temperature thresholds

All 19 subjects described 39°C as a warm to hot sensation, the 43°C stimulus was considered hot to slightly painful, and 46°C evoked a strong burning sensation in all volunteers during WDT and HPT determination as well as after test heat stimulation. WDT in all 19 subjects was 3.0 ± 0.56 and 2.1 ± 0.17°C (arithmetic mean ± standard error) in the V1 and V3 area, respectively. HPT was 42.3 ± 0.82°C (V1) and 41.8 ± 0.7°C (V3).

fMRI data

Due to strong movements one subject was excluded from further data analysis. Thus the following data analyses were based upon 18 experiments in 18 volunteers.

Single subject analysis

Results of 18 subjects based upon a minimum cluster size of 3 voxel [3 × (1.09 × 1.09 × 3 mm^3) = 10.7 mm^3] and $P < 0.02$ ($T > 2.06$) for activation in the pons and $P < 0.05$ ($T > 1.65$) for activation in the medulla and SDH. In order to avoid bias of activation in the group analysis, which is caused by only a few individual BOLD signal changes, the results of the respective single subject analyses were carefully inspected. Corresponding to the localization of the STN, only clusters localized in the SDH, medulla oblongata or pons and in the dorsolateral quadrant within the axial section were included in the data analyses. During V1 stimulation, bilateral activation in the brainstem was detected in 13 out of 18 volunteers throughout application of 46°C. During stimulation with 43 and 39°C, bilateral brainstem activation occurred in 10 and 12 subjects, respectively. During thermal stimulation with 39, 43, and 46°C in the V3 area, bilateral brainstem activation was recorded in 10, 11, and 12 subjects, respectively (for examples of activation in single subject analysis cf. Fig. 3). Statistical analysis of temperature dependency (number of cluster and voxel) and differences between V1 and V3 stimulation did not show any significant effects (ANOVA).

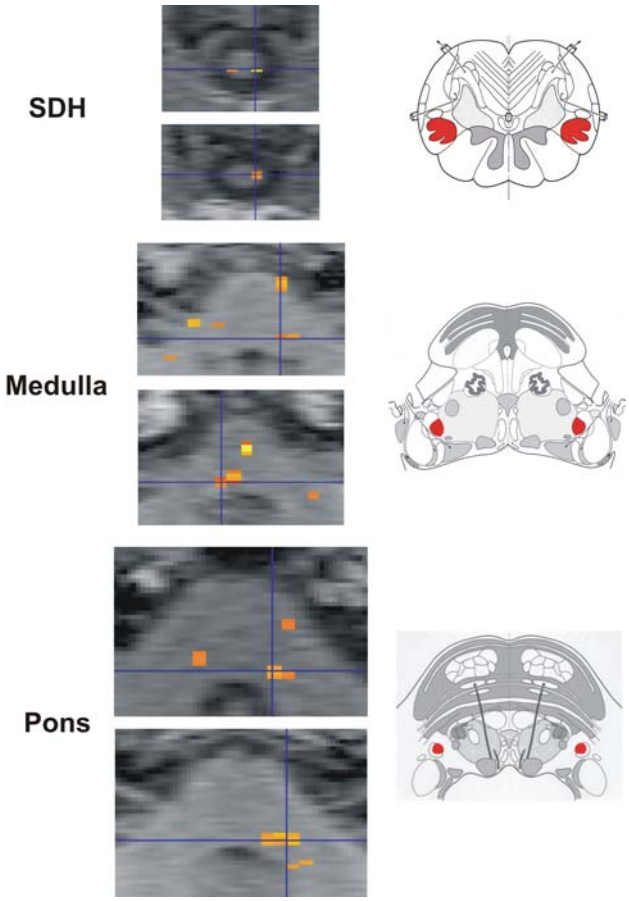

Fig. 3 Example of brainstem activations due to temperature stimulation in single subject analysis. Axial sections of the SDH, medulla, and pons on the left side are shown in comparison to the anatomical STN site given by two atlases on the right side (*red/dark gray* STN). *Blue/Gray crosslines* show focus on major interest activation clusters. All temperatures were included (39, 43, 46°C), $n = 1$, V1 and V3, uncorrected $P \leq 0.02/0.05$, $T > 2.06/1.65$ (3/1, 2). Anatomical drawings modified from Duvernoy [15] and DeArmond et al. [12]

Group analysis

The above described approach of fMRI data processing (Fig. 2a, b) with a combination of different analyzing programs and a procedure to generate a 3D brainstem template enabled group analysis of functional brainstem data.

Functional data at all temperatures were analyzed with a minimal bottom line significance of $P < 0.01$ corresponding to $T > 2.8$ (BrainVoyager GLM, RE, ANOVA). Positive and negative BOLD signals and temperature contrasts

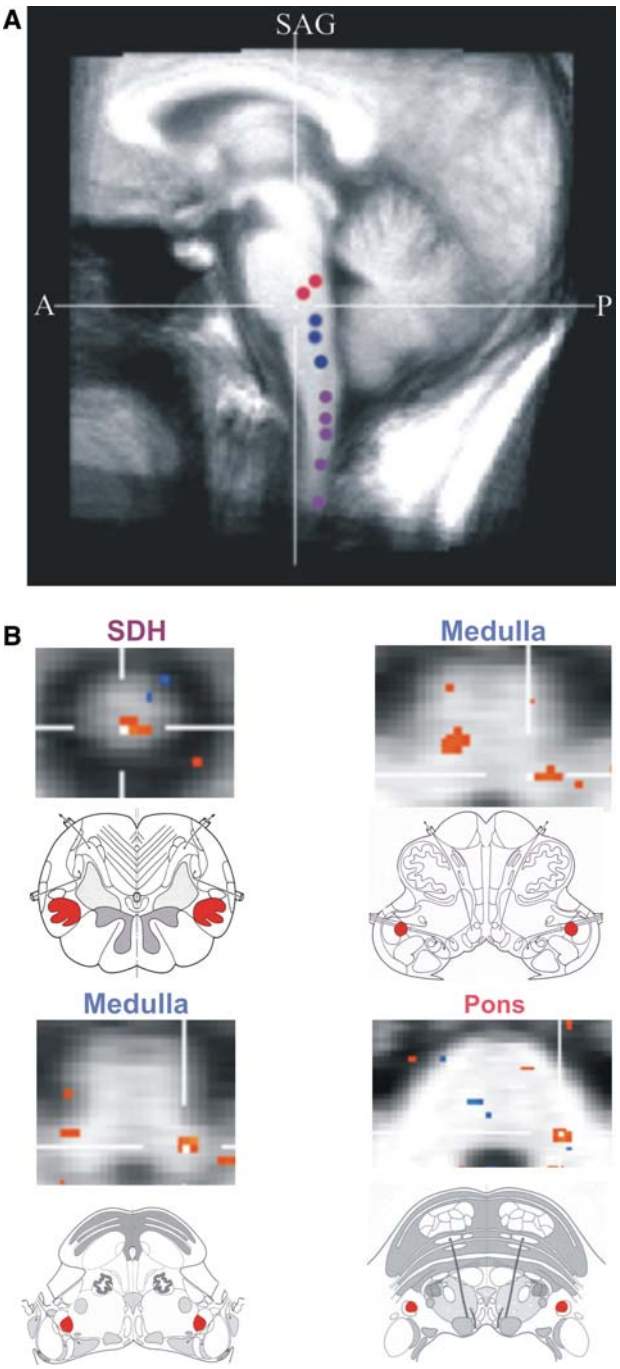

Fig. 4 Examples of brainstem activation due to temperature stimulation in group analysis. All temperatures were included (39, 43, 46°C), $n = 18$, V1 and V3, uncorrected $P \leq 0.01$. Displayed data are the results of the matching of localizations (cf. "Matching of localizations"). **a**. Anatomical template with activation clusters. Median-sagittal section of the template shows the localization of the ten activation clusters in the brainstem obtained by the matching of localizations. Activation is located columnar in the dorsolateral quadrant of the brainstem. The *different colors* encode for different anatomical levels [SDH (*purple/light gray*), medulla (*blue/dark gray*), pons (*red/light gray*)]. **b** Selected slices showing activation in SDH, medulla, and pons. Transverse sections displaying group activation in comparison to the STN localization given by two atlases (*marked red/dark gray* STN). Sections arranged from caudal (*top row*, *left side*) to rostral (*bottom row*, *right side*). Bilateral activation can be seen in the two pictures at medullary level. Anatomical drawings modified from Duvernoy [15] and DeArmond et al. [12]

as well as single temperatures were taken into account. With a minimum cluster size of 2 voxel [$2 \times (1 \times 1 \times 1\ mm^3) = 2\ mm^3$], significant activation ($P < 0.01$, $T > 2.8$) was found within the dorsolateral brainstem in ten matched localizations distributed over the SDH, pons, and medulla oblongata (Fig. 4). Most clusters at single temperatures and temperature contrasts were located in these ten sites. Activation not matching the sites was excluded from data analysis. Ipsilateral and contralateral clusters showed similar sizes and contained approx. 2–10 voxel (fewer numbers of voxel in the SDH, increased numbers in the pons). Bilateral activations occurred during V1 as well as V3 stimulation. Still, differences in stimuli processing could be found: contralateral activation was present more frequently during V1 stimulation in comparison to V3. Considering the matching of localizations, ipsilateral and contralateral positive BOLD signals occurred at a ratio of 5/5 (No. of clusters ipsilateral/contralateral) during V1 stimulation, whereas V3 input evokes a ratio of 7/2 (all temperatures included, only positive BOLD signals, $n = 18$, GLM, RE, ANOVA, uncorrected $P \leq 0.01$, $T > 2.8$).

Mental and supraorbital heat stimulation led to activation in different areas within the brainstem. Noxious input to the V1 area caused increased activation in caudal parts within the STN region (SDH and junction SDH/medulla), whereas V3 stimulation elicited BOLD signals in rostral parts (pons and pontomedullary junction). During V1 stimulation, 5 clusters (26%) were found in caudal and 5 (26%) in rostral parts within the brainstem. Regarding V3, the majority of activation (6 clusters, 32%) was located in the rostral STN area, whereas 3 (16%) were in the caudal division (all temperatures included, only positive BOLD signals, $n = 18$, GLM, RE, ANOVA, uncorrected $P \leq 0.01$, $T > 2.8$).

Regarding temperature correlation, at 39, 42 and 46°C, 0, 1, and 8 clusters were detected after V3 and 3, 2 and 5 cluster after V1 stimulation, respectively (statistics of positive BOLD signals, $n = 18$, GLM, RE, ANOVA, uncorrected $P \leq 0.01$, $T > 2.8$). Statistical analysis showed no significant correlation between temperature and brainstem activation.

Discussion

The human experimental study revealed bilateral activity in the spinal trigeminal nucleus due to unilateral heat stimulation of the face in healthy volunteers. Sensory input from

V1 more frequently induced contralateral brainstem activation than noxious input from V3. Stimulation of V1 or V3 evoked ipsilateral activity in caudal or rostral areas of STN, respectively.

Due to the non-invasiveness, general availability, and standardized analysis algorithms, a large number of studies on pain-induced brain activation have been performed using fMRI in the last decade. However, most focused on signal processing in the cortex, while the number of corresponding studies of the brainstem is limited. So far, there is no common template for the human brainstem. Imaging studies focusing on neural processing in cortical brain areas usually apply standard brains from the Montreal Neurological Institute (MNI, www.bic.mni.mcgill.ca) and the Talairach atlas [53]. Former studies often presented individual brainstem data [11]. Nonetheless, a group analysis could not be performed and might be helpful when investigating larger populations. A group analysis would possibly create further insights into brainstem processing according to the progress in cortical neuroscience facilitated by appropriate fMRI techniques in the last decade. Some projects recently addressed that problem [6, 14, 31, 36, 40]; however, a gold standard is still missing. The present study demonstrated an algorithm of data processing that enables the projection of brainstem activity onto a standardized 3D space. The algorithm provides the ability to show precise activation localization without affecting the data's reliability and accuracy.

In order to obtain higher data quality and to minimize false positive activation, single-shot multi-echo sequences [47], sagittal slices [54, 62], a small field of view without cortex and regional shimming [54] were applied. Sagittal slices may cause reduced through-plane resolution but still it enables a good FOV overview with only minor artifacts and distortion. According to current literature, no smoothing was carried out in group analysis [54]. Throughout GLM group analysis, a z-transformation was applied onto the whole time course to allow for a dissociation of the time axis and an equilibration of signal level. In the single subject analysis and the group analysis, different quality criteria were applied. In order to detect any significant activation in the single subject analysis, P values were set to $P < 0.02$ ($T > 2.06$) for activation in the pons and $P < 0.05$ ($T > 1.65$) for activation in the medulla and the SDH with a minimum cluster size of 3 voxel [$3 \times (1.09 \times 1.09 \times 3\ \mathrm{mm}^3) = 10.7\ \mathrm{mm}^3$] [11, 36]. The group analysis applied a higher level of significance with $P < 0.01$ ($T > 2.8$) and a minimum cluster size of 2 mm^3. Since cardiac- and breathing-gated fMRI was not available [46, 54, 65], a high-pass filter was applied during post-processing to minimize possible artifacts [65]. With this, low-frequency noise was minimized and data did not show any uniform repetitive signals which might correspond to cardiac or respiratory artifacts. Exclusion of brainstem movement >3 mm/3° and realignment minimized false positive activation. By applying normalization onto brainstem data, group results with further data analysis could be achieved. The present experiment revealed positive as well as negative changes in BOLD signals. Deactivation at the brainstem level has been described previously [3, 5, 36], but their origin cannot sufficiently be explained [20, 37]. According to other studies, the present experiment mainly focused on positive BOLD changes.

Pain processing was visualized in the human brainstem previously [36, 41, 45]. Bilateral processing at the brainstem has not yet been addressed although ipsilateral and contralateral projections of trigeminal afferent input was demonstrated at the thalamic and cortical levels [4, 18, 22, 26, 41]. Bilateral fMRI signals were detected during V1 as well as V3 stimulation. This is very likely a reliable phenomenon and is supported by bilateral activity in single subject and group analyses. The accuracy of the present data is supported by the following facts. As the STN is columnarly situated in the dorsolateral quadrant of the brainstem [1, 7, 15, 64], only activation meeting these criteria was included. The correct cluster position was verified by two distinct analyzing steps. During single subject analysis, a direct comparison of clusters was performed by overlaying neuroanatomical drawings [12, 15] onto the axial slices of activation in question and only those located in the specified area were included in the analysis. During group analysis, a detailed comparison between the location of the clusters and the atlas ensured strict containment to the STN area (Fig. 4). As a consequence, the matching of localization showed constantly reappearing activation sites even at different temperatures or subjects and therefore confirms the reliability of data. Applied statistics ensured a high level of significance to the results ($P < 0.01$, $T > 2.8$, BrainVoyager GLM, RE, ANOVA).

Contralateral activation might be due to primary afferents, projections from the contralateral STN, or a combination of both. Histological studies from rodents provided evidence for V1 as well as V3 primary afferent projections to contralateral STN [23–25, 38, 60, 61]. Projections between bilateral STN were also detected for both divisions [2, 17, 21, 23, 43].

The presented results indicate increased contralateral activation during V1 stimulation in comparison to V3 stimulation, which corresponds to evidence from rodents. Various histological studies showed V3 contralateral projections [25, 38, 52, 59], whereas V1 primary afferents have been studied less frequently. Afferent fiber tracts seem to be more distinctive in this division [16, 23, 39, 44]. Bilateral processing of V1 stimuli in the somatosensory cortex were found in human subjects, whereas V3 stimulation evoked only unilateral activity [22].

In atypical Wallenberg syndrome, contralateral and bilateral facial hypesthesia can be found [8, 28–30, 35, 51, 56]. If patients have more afflictions on the ipsilateral side, the contralateral sides of their face might be examined less. Some studies propose that an affection of the trigeminothalamic tract in large infarctions might account for hypesthesia on the contralateral face [10, 57]. However, this is not always the case [8, 28]. On the other hand, input from the contralateral face may cause these symptoms as well. Unilateral noxious low-frequency stimulation in human subjects showed bilateral long-term depression of the trigemino-facial blink reflex [63]. This might be based upon bilateral projections of nociceptive afferents onto STN neurons.

The present data indicate a spatial organization of brainstem activation within the STN. V1 signals were located more caudally within the brainstem, whereas V3 stimuli evoked activity in more rostral parts within the STN. This may correspond to a somatotopic organization within STN as described in the literature [11, 13, 19, 48–50].

This fMRI study suggests bilateral brainstem activation during thermal stimulation of human facial skin. A new method of analyzing fMRI data at the brainstem level might account for improved data interpretation in the future. In addition, technical progress might assist in displaying the STN region more accurately.

Acknowledgments This work was supported by the Interdisciplinary Center for Clinical Research at RWTH Aachen University. This paper is part of the doctoral thesis of cand. med. Bärbel Kubina at the Medical Faculty of RWTH Aachen University.

References

1. Afshar F, Dykes E (1984) Computer-generated three-dimensional visualization of the trigeminal nuclear complex. Surg Neurol 22:189–196
2. Arends JJ, Woelders-Blok A, Dubbeldam JL (1984) The efferent connections of the nuclei of the descending trigeminal tract in the mallard (*Anas platyrhynchos* L.). Neuroscience 13:797–817
3. Becerra L, Breiter HC, Wise R, Gonzalez RG, Borsook D (2001) Reward circuitry activation by noxious thermal stimuli. Neuron 32:927–946
4. Becerra L, Morris S, Bazes S, Gostic R, Sherman S, Gostic J, Pendse G, Moulton E, Scrivani S, Keith D, Chizh B, Borsook D (2006) Trigeminal neuropathic pain alters responses in CNS circuits to mechanical (brush) and thermal (cold and heat) stimuli. J Neurosci 26:10646–10657
5. Borsook D, DaSilva AF, Ploghaus A, Becerra L (2003) Specific and somatotopic functional magnetic resonance imaging activation in the trigeminal ganglion by brush and noxious heat. J Neurosci 23:7897–7903
6. Capozza M, Iannetti GD, Mostarda M, Cruccu G, Accornero N (2000) Three-dimensional mapping of brainstem functional lesions. Med Biol Eng Comput 38:639–644
7. Carpenter MB, Sutin J (1983) Human neuroanatomy. Williams & Wilkins, Baltimore
8. Chia LG, Shen WC (1993) Wallenberg's lateral medullary syndrome with loss of pain and temperature sensation on the contralateral face: clinical, MRI and electrophysiological studies. J Neurol 240:462–467
9. Clara M (1959) Das Nervensystem des Menschen. Johann Ambrosius Barth Verlag, Leipzig
10. Conforto AB, Yamamoto FI, Leite CC, Scaff M, Marie SK (2005) Facial sensory symptoms in medullary infarcts. Arq Neuropsiquiatr 63:946–950
11. DaSilva AF, Becerra L, Makris N, Strassman AM, Gonzalez RG, Geatrakis N, Borsook D (2002) Somatotopic activation in the human trigeminal pain pathway. J Neurosci 22:8183–8192
12. DeArmond SJ, Dewey MM, Fusco MM (1989) Structure of the human brain: a photographic atlas. Oxford University Press, USA
13. Dejerine J (1914) Semiologie des Affections Du Systeme Nerveau. Masson et Cie, Paris
14. Diedrichsen J (2006) A spatially unbiased atlas template of the human cerebellum. NeuroImage 33:127–138
15. Duvernoy HM (1995) The human brain stem and cerebellum. Springer, New York
16. Ellrich J, Messlinger K (1999) Afferent input to the medullary dorsal horn from the contralateral face in rat. Brain Res 826:321–324
17. Falls WM (1984) The morphology of neurons in trigeminal nucleus oralis projecting to the medullary dorsal horn (trigeminal nucleus caudalis): a retrograde horseradish peroxidase and Golgi study. Neuroscience 13:1279–1298
18. Fitzek S, Fitzek C, Huonker R, Reichenbach JR, Mentzel HJ, Witte OW, Kaiser WA (2004) Event-related fMRI with painful electrical stimulation of the trigeminal nerve. Magn Reson Imaging 22:205–209
19. Gerebtzoff MA (1975) Location and somatotopic organization of visceromotor, motor and sensory columns of the cranial nerves. Acta Otorhinolaryngol Belg 29:873–888
20. Harel N, Lee SP, Nagaoka T, Kim DS, Kim SG (2002) Origin of negative blood oxygenation level-dependent fMRI signals. J Cereb Blood Flow Metab 22:908–917
21. Hockfield S, Gobel S (1982) An anatomical demonstration of projections to the medullary dorsal horn (trigeminal nucleus caudalis) from rostral trigeminal nuclei and the contralateral caudal medulla. Brain Res 252:203–211
22. Iannetti GD, Porro CA, Pantano P, Romanelli PL, Galeotti F, Cruccu G (2003) Representation of different trigeminal divisions within the primary and secondary human somatosensory cortex. Neuroimage 19:906–912
23. Jacquin MF, Chiaia NL, Rhoades RW (1990) Trigeminal projections to contralateral dorsal horn: central extent, peripheral origins, and plasticity. Somatosens Mot Res 7:153–183
24. Jacquin MF, Semba K, Egger MD, Rhoades RW (1983) Organization of HRP-labeled trigeminal mandibular primary afferent neurons in the rat. J Comp Neurol 215:397–420
25. Jacquin MF, Semba K, Rhoades RW, Egger MD (1982) Trigeminal primary afferents project bilaterally to dorsal horn and ipsilaterally to cerebellum, reticular formation, and cuneate, solitary, supratrigeminal and vagal nuclei. Brain Res 246:285–291
26. Jantsch HH, Kemppainen P, Ringler R, Handwerker HO, Forster C (2005) Cortical representation of experimental tooth pain in humans. Pain 118:390–399
27. Kameda W, Kawanami T, Kurita K, Daimon M, Kayama T, Hosoya T, Kato T (2004) Lateral and medial medullary infarction: a comparative analysis of 214 patients. Stroke 35:694–699
28. Kim JS (2003) Pure lateral medullary infarction: clinical-radiological correlation of 130 acute, consecutive patients. Brain 126:1864–1872
29. Kim JS, Choi-Kwon S (1999) Sensory sequelae of medullary infarction: differences between lateral and medial medullary syndrome. Stroke 30:2697–2703

30. Kim JS, Lee JH, Lee MC (1997) Patterns of sensory dysfunction in lateral medullary infarction. Clinical-MRI correlation. Neurology 49:1557–1563
31. Komisaruk BR, Mosier KM, Liu WC, Criminale C, Zaborszky L, Whipple B, Kalnin A (2002) Functional localization of brainstem and cervical spinal cord nuclei in humans with fMRI. AJNR Am J Neuroradiol 23:609–617
32. Kubina B, Ristic D, Weber J, Stracke CP, Ellrich J (2007) Bilateral brainstem activation by noxious thermal stimulation in the face. Clin Neurophysiol 118:2810–2811
33. LaMotte RH, Campbell JN (1978) Comparison of responses of warm and nociceptive C-fiber afferents in monkey with human judgments of thermal pain. J Neurophysiol 41:509–528
34. Lancaster JL, Tordesillas-Gutierrez D, Martinez M, Salinas F, Evans A, Zilles K, Mazziotta JC, Fox PT (2007) Bias between MNI and Talairach coordinates analyzed using the ICBM-152 brain template. Hum Brain Mapp 28:1194–1205
35. MacGowan DJ, Janal MN, Clark WC, Wharton RN, Lazar RM, Sacco RL, Mohr JP (1997) Central poststroke pain and Wallenberg's lateral medullary infarction: frequency, character, and determinants in 63 patients. Neurology 49:120–125
36. Mainero C, Zhang WT, Kumar A, Rosen BR, Sorensen AG (2007) Mapping the spinal and supraspinal pathways of dynamic mechanical allodynia in the human trigeminal system using cardiac-gated fMRI. Neuroimage 35:1201–1210
37. Malonek D, Grinvald A (1996) Interactions between electrical activity and cortical microcirculation revealed by imaging spectroscopy: implications for functional brain mapping. Science 272:551–554
38. Marfurt CF (1981) The central projections of trigeminal primary afferent neurons in the cat as determined by the tranganglionic transport of horseradish peroxidase. J Comp Neurol 203:785–798
39. Marfurt CF, Rajchert DM (1991) Trigeminal primary afferent projections to "non-trigeminal" areas of the rat central nervous system. J Comp Neurol 303:489–511
40. Marx JJ, Iannetti GD, Thoemke F, Fitzek S, Galeotti F, Truini A, Stoeter P, Dieterich M, Hopf HC, Cruccu G (2008) Topodiagnostic implications of hemiataxia: an MRI-based brainstem mapping analysis. Neuroimage 39:1625–1632
41. Moulton EA, Pendse G, Morris S, Strassman A, iello-Lammens M, Becerra L, Borsook D (2007) Capsaicin-induced thermal hyperalgesia and sensitization in the human trigeminal nociceptive pathway: an fMRI study. Neuroimage 35:1586–1600
42. Nieuwenhuys R, Voogd J, van Huijzen C (2008) The human central nervous system. Springer, Berlin
43. Panneton WM, Burton H (1982) Origin of ascending intratrigeminal pathways in the cat. Brain Res 236:463–470
44. Panneton WM, Klein BG, Jacquin MF (1991) Trigeminal projections to contralateral dorsal horn originate in midline hairy skin. Somatosens Mot Res 8:165–173
45. Petrovic P, Petersson KM, Hansson P, Ingvar M (2004) Brainstem involvement in the initial response to pain. Neuroimage 22:995–1005
46. Poncelet BP, Wedeen VJ, Weisskoff RM, Cohen MS (1992) Brain parenchyma motion: measurement with cine echo-planar MR imaging. Radiology 185:645–651
47. Posse S, Wiese S, Gembris D, Mathiak K, Kessler C, Grosse-Ruyken ML, Elghahwagi B, Richards T, Dager SR, Kiselev VG (1999) Enhancement of BOLD-contrast sensitivity by single-shot multi-echo functional MR imaging. Magn Reson Med 42:87–97
48. Price DD, Dubner R, Hu JW (1976) Trigeminothalamic neurons in nucleus caudalis responsive to tactile, thermal, and nociceptive stimulation of monkey's face. J Neurophysiol 39:936–953
49. Shigenaga Y, Chen IC, Suemune S, Nishimori T, Nasution ID, Yoshida A, Sato H, Okamoto T, Sera M, Hosoi M (1986) Oral and facial representation within the medullary and upper cervical dorsal horns in the cat. J Comp Neurol 243:388–408
50. Shigenaga Y, Okamoto T, Nishimori T, Suemune S, Nasution ID, Chen IC, Tsuru K, Yoshida A, Tabuchi K, Hosoi M (1986) Oral and facial representation in the trigeminal principal and rostral spinal nuclei of the cat. J Comp Neurol 244:1–18
51. Smith DB, Demasters BK (1981) Demyelinating disease presenting as Wallenberg's syndrome. Report of a patient. Stroke 12:877–878
52. Takemura M, Sugimoto T, Sakai A (1987) Topographic organization of central terminal region of different sensory branches of the rat mandibular nerve. Exp Neurol 96:540–557
53. Talairach J, Tournoux P (1988) Co-planar stereotaxic atlas of the human brain. Thieme, Stuttgart
54. Tracey I, Iannetti GD (2006) Brainstem functional imaging in humans. Suppl Clin Neurophysiol 58:52–67
55. Treede R-D, Meyer RA, Raja SN, Campbell JN (1995) Evidence for two different heat transduction mechanisms in nociceptive primary afferents innervating monkey skin. J Physiol 483:747–758
56. Valls-Sole J, Vila N, Obach V, Alvarez R, Gonzalez LE, Chamorro A (1996) Brain stem reflexes in patients with Wallenberg's syndrome: correlation with clinical and magnetic resonance imaging (MRI) findings. Muscle Nerve 19:1093–1099
57. Vuilleumier P, Bogousslavsky J, Regli F (1995) Infarction of the lower brainstem clinical, aetiological and MRI-topographical correlations. Brain 118(Pt 4):1013–1025
58. Wallenberg A (1895) Acute bulbar affection. Arch Psychiatr Nervenkr 27:504–540
59. Westrum LE, Canfield RC (1977) Electron microscopy of degenerating axons and terminals in spinal trigeminal nucleus after tooth pulp extirpations. Am J Anat 149:591–596
60. Westrum LE, Henry MA (1991) Contralateral degeneration in the cat spinal trigeminal nucleus following unilateral retrogasserian trigeminal rhizotomy. Neurosci Lett 121:143–146
61. Westrum LE, Henry MA (1993) Unilateral retrogasserian rhizotomy causes contralateral degeneration in spinal trigeminal nuclei of cats: an ultrastructural study. Exp Brain Res 93:28–36
62. Wilmink JT, Backes WH, Mess WH (2003) Functional MRI of the spinal cord: will it solve the puzzle of pain? JBR BTR 86:293–294
63. Yekta SS, Lamp S, Ellrich J (2006) Heterosynaptic long-term depression of craniofacial nociception: divergent effects on pain perception and blink reflex in man. Exp Brain Res 170:414–422
64. Young RF, Perryman KM (1984) Pathways for orofacial pain sensation in the trigeminal brain-stem nuclear complex of the Macaque monkey. J Neurosurg 61:563–568
65. Zhang WT, Mainero C, Kumar A, Wiggins CJ, Benner T, Purdon PL, Bolar DS, Kwong KK, Sorensen AG (2006) Strategies for improving the detection of fMRI activation in trigeminal pathways with cardiac gating. Neuroimage 31:1506–1512